International Journal of Heat and Fluid Flow xxx (2009) xxx–xxx

Contents lists available at ScienceDirect

International Journal of Heat and Fluid Flow

journal homepage: www.elsevier.com/locate/ijhff

Accurate heat transfer measurements using thermochromic liquid crystal. Part 2: Application to a rotating disc

V.U. Kakade, G.D. Lock *, M. Wilson, J.M. Owen, J.E. Mayhew [1]

Department of Mechanical Engineering, University of Bath, Bath, BA2 7AY, England, United Kingdom

ARTICLE INFO

Article history:
Received 26 August 2008
Received in revised form 10 March 2009
Accepted 7 April 2009
Available online xxxx

Keywords:
Transient heat transfer
Thermochromic liquid crystal
Rotating flow

ABSTRACT

Encapsulated thermochromic liquid crystal (TLC) can accurately measure surface temperature in a variety of heat transfer and fluid-flow experiments. In Part 1 of this two-part paper, two narrow-band liquid crystals were specifically calibrated for application to experiments on a disc rotating at high speed (~5000 rpm). Part 2 describes how these crystals were used to measure the surface temperature on the disc in a transient experiment that models the flow of internal cooling air in a gas turbine. The TLC was viewed through the transparent polycarbonate disc using a digital video camera and strobe light synchronised to the disc frequency. The convective heat transfer coefficient, h, was subsequently calculated from the one-dimensional solution of Fourier's conduction equation for a semi-infinite wall. The analysis accounted for the exponential rise in the air temperature driving the heat transfer, and for experimental uncertainties in the measured values of h. The paper focuses on the method used, and sample experimental results are provided to demonstrate the accuracy and potency of the technique.

1. Introduction

The use of thermochromic liquid crystal (TLC) in heat transfer experiments is a well-established practice; Ireland and Jones (2000) and Baugh (1995) provide reviews of how the technology has been utilised in a range of fluid-flow applications. In a transient experiment, each site on the TLC surface will change colour through the optically-active temperature range and this process is captured digitally. If the time at which the TLC changes colour is known (so that the surface temperature is also known) then the heat transfer coefficient, h, can be calculated from the one-dimensional solution of Fourier's conduction equation for a semi-infinite wall. Schultz and Jones (1973) provide an analytical solution for a *step-change* in the air (or convective fluid) temperature. In some experiments it is not possible to create a step-change, due to (for example) thermal inertia upstream of the test section. Such cases, which the authors have experienced in their own experiments, are referred to here as *slow transients*. For the special case where the air temperature rises exponentially with time, Gillespie et al. (1998) obtained an analytical solution of Fourier's equation. This solution was extended to an exponential-series technique by Newton et al. (2003), who demonstrated that the accuracy of the simple step-change method could be brought to the more difficult case of the slow transient.

Uncertainties in the measured temperatures give rise to uncertainties in the calculated values of h, and a means of estimating and minimising these uncertainties for the step-change solution of Fourier's equation is given by Yan and Owen (2002); this analysis was extended to the slow transient case by Owen et al. (2003). Another source of error is lateral conduction: the one-dimensional analysis considers only the conduction in the direction normal to the surface of the wall, and conduction in the transverse directions is ignored. Kingsley-Rowe et al. (2005) provide an analytical correction that can be used when lateral conduction is significant.

The object of Part 2 of this two-part paper is to demonstrate the application of the TLC techniques developed in Part 1 to a heat transfer case of particular interest to the gas-turbine community: pre-swirl flow in a rotating-disc system. As well as being important to the designers of internal-air systems, it raises experimental difficulties over and above those found in stationary systems.

It is not the object of this paper to discuss the fundamentals of rotating flows, and the interested reader is referred to Owen and Rogers (1989) if more details are required. Suffice it to say that the flow structures encountered in the experiments discussed below correspond to a rotor–stator system where the gap between the discs and the rotational Reynolds number are large enough to ensure turbulent flow and separate boundary layers. It is also not the object to describe in detail the flow and heat transfer in pre-swirl systems.

In principle, infra-red (IR) imaging could be used instead of TLC for rotating systems (see, for example, Cardone et al., 1997; Dryer et al., 2005; Mori et al., 2007; Pellé and Harmand, 2007). IR has the advantage that the temperature can be measured accurately over a wide-range, while TLC only provides measurements of temperature in its active range. However, apart from the expense of the IR

* Corresponding author. Tel.: +44 1225 386854.
E-mail address: ensgdl@bath.ac.uk (G.D. Lock).
[1] Present address: Rose-Hulman Institute of Technology, IN, USA.

0142-727X/$ - see front matter © 2009 Elsevier Inc. All rights reserved.
doi:10.1016/j.ijheatfluidflow.2009.04.005

Nomenclature for Parts 1 and 2

a	rotor inner radius
b	rotor outer radius
Bi	Biot number based on film thickness = $h\delta x/k$
c	specific heat
c_j	weighting term in exponential series
c_w	non-dimensional mass flow rate ($= \dot{m}/\mu b$)
C	cycle number
$g\ (\beta, \beta_\tau)$	slow-transient solution of Fourier's equation = $g(\beta, \lambda)$
h	heat transfer coefficient (= $q_w/(T_{aw} - T_w)$)
H	hue
k	thermal conductivity
q_w	heat flux from air to wall
m	number of terms in exponential series
$\dot{m}$	mass flow rate
P	uncertainty (95% confidence estimate)
$(Re_\phi$	rotational Reynolds number (= $\rho\Omega b^2/\mu$)
r	radius
r_p, r_b	radii of pre-swirl nozzles and receiver holes
R	probe recovery factor
RGB	red, green, blue intensities
s	rotor–stator separation distance
S_c	seal clearance
t	time
T	temperature
$T_a(t)$	total-temperature of air
$T_{aw}(t)$	adiabatic-wall temperature
T_e	copper block temperature
T_{tc}	temperature measured by thermocouple
$T_w(t)$	surface temperature of wall
V	air velocity when calibrating total-temperature probe
β	nondimensional heat transfer coefficient = $(h\sqrt{t/\kappa})$ based on time
β_τ	nondimensional heat transfer coefficient = $(h\sqrt{\tau/\kappa})$ based on time-constant
β_p	swirl ratio (=$V_\varphi/\Omega r$)
δx	effective thickness of TLC film
κ	thermal diffusivity of plate = ρck
ζ	normalised temperature for calibration
θ	relative lighting and viewing angle
Θ	non-dimensional temperature in solution to Fourier's eq. = $\frac{T_w - T_0}{T_{aw,\infty} - T_0}$
λ	non-dimensional parameter = $\sqrt{t/\tau}$
λ_T	turbulent-flow parameter ($= c_w Re_\phi^{-0.8}$)
μ	dynamic viscosity
ρ	density
τ	time constant
Φ_h^*	amplification parameter for uncertainty in h
Ω	angular velocity of rotor

Subscripts

0	value at $t = 0$
j	term in exponential series
M	median value
min	minimum value
o	overall
R, G, B	red, green, blue
φ	circumferential direction

imaging equipment, viewing through stationary or rotating windows requires the use of special materials (such as zircon or germanium) with transmission losses that require careful calibration; the calibration is further complicated when it is not possible to achieve black-body radiation from the surfaces of interest. By using a stroboscope, and with TLC sprayed in segments on the rotating and stationary discs, it is possible to determine simultaneously the heat transfer on both discs; this would be impracticable with IR thermography.

This paper describes the application of TLC to measure the heat transfer coefficient on a rotating disc in a test facility which models the cooling flow in a modern gas turbine. In the experiments, two narrow-band TLC (each active over 1 °C) were viewed through a transparent polycarbonate disc (acting as a semi-infinite substrate). A strobe light, synchronised to the disc rotation, was used to illuminate the crystals, and black paint (to enhance the colour contrast) was applied to the side exposed to the hot gas. In Section 2 the apparatus used to generate the experimental data and the thermal boundary conditions are described. Section 3 summarises the analytical solution to Fourier's equation for a slow transient and the analytical method of calculating the uncertainty in h; further details appear in Appendix A. The procedure to determine a temperature–time pair at each measurement point on the disc is described in Section 4. Section 5 illustrates examples of the measured data and an interpretation in terms of the fluid dynamics governing the convective heat transfer. The conclusions are presented in Section 6.

2. Experimental apparatus

Experiments were conducted using a simplified model of a gas-turbine rotor–stator system. The geometry, which was based on information obtained for existing engine designs, is illustrated schematically in Fig. 1a and b. Air entered the test section through the stator at low radius via pre-swirl nozzles and flowed radially outward between the rotating disc and the stator, exiting through 60 axial receiver holes in the disc representing the entrance to blade-cooling passages in the engine. The air was heated, upstream of the nozzles, by a mesh heater (see Lock et al., 2004) which created a step-change in the air temperature.

Karabay et al. (2001) have shown that for turbulent pre-swirl flow in rotating cavities, where the gap ratio is large enough to ensure separate boundary layers, the swirling flow is governed principally by two nondimensional variables: the pre-swirl ratio, β_p, and the turbulent-flow parameter, $\lambda_T = C_w Re_\varphi^{-0.8}$; the latter combines the effects of the nondimensional pre-swirl flow rate, C_w, and the rotational Reynolds number, Re_φ, for the disc. The fluid dynamics of this facility has been investigated both experimentally and computationally by Yan et al. (2003). The mass flow rates and disc rotational speed (typically 5000 rpm) were chosen to simulate engine-representative values of β_p and λ_T and hence the flow structure is considered to be representative of that found in cooling systems of engines (Owen and Rogers, 1989). The geometric properties of the test rig and the range of operating conditions are summarised in Table 1.

Local heat transfer coefficients on the rotating disc were determined from transient surface-temperature measurements using the two calibrated narrow-band TLC (designated as 30 and 40 °C to indicate their activation temperatures). The experiments were conducted under known thermal boundary conditions, using air which had been pre-heated to approximately 50 °C using the mesh heater upstream of the pre-swirl nozzles. As discussed in Section 4, the method relied on the accurate measurement of the time taken for the 30 and 40 °C crystals on the rotor surface to reach a unique value of hue, which had been accurately calibrated against temper-

Please cite this article in press as: Kakade, V.U., et al. Accurate heat transfer measurements using thermochromic liquid crystal. Part 2: Application to a rotating disc. Int. J. Heat Fluid Flow (2009), doi:10.1016/j.ijheatfluidflow.2009.04.005

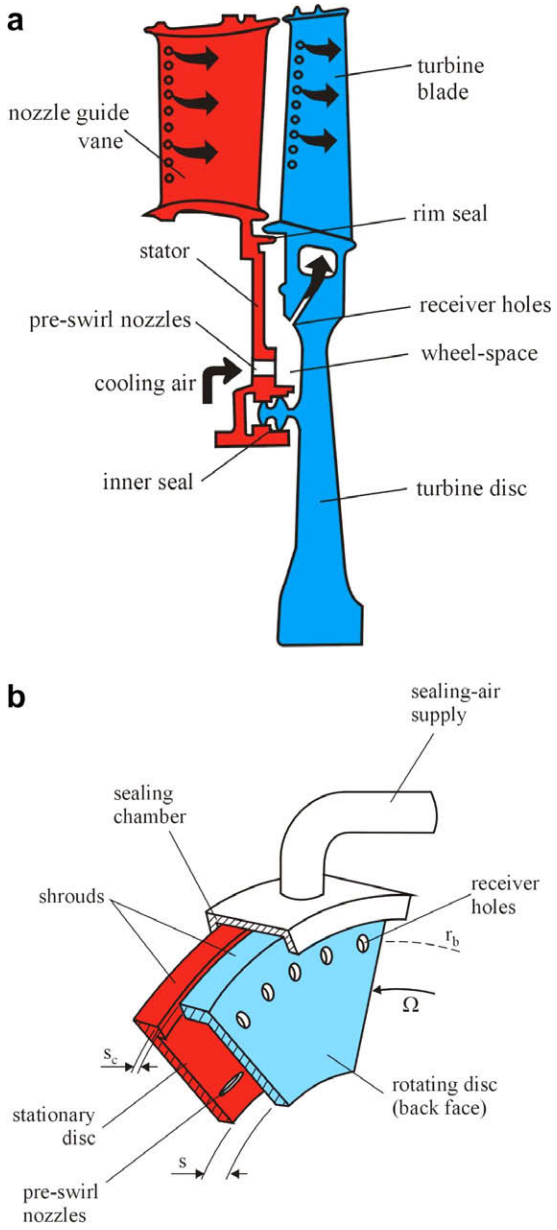

Fig. 1. (a) Typical gas-turbine rotor–stator system with pre-swirled cooling air; (b) simplified model of rotor–stator system.

Table 1
Summary of geometry and operating conditions.

Disc outer radius, b	216 mm
Inner radius, a	$a/b = 0.67$
Gap ratio	$s/b = 0.051$
Pre-swirl radius, r_p	$r_p/b = 0.74$
Receiver-hole radius, r_b	$r_b/b = 0.93$
Re_φ	0.78×106–1.2×106
λ_T	0.125–0.36
β_p	0.5–1.5
C_w	6600–27200

ature. The crystals were sprayed on the disc in sectors inside the wheel-space, which could be viewed through the transparent polycarbonate by a digital video camera. As in the calibration, the thickness of the TLC film was 45 μm and a thin (~5 μm) layer of black paint was used to provide contrast to the colour of the TLC. The thermal properties of polycarbonate: $\rho = 1200$ kg/m^3, $k = 0.19$ W/m K, and $c = 1200$ J/kg K.

Fig. 2 is a colour image selected from a time sequence obtained by the digital camera during a typical experiment. This image shows the activated TLC as viewed through the transparent polycarbonate rotor, rotating clockwise in this view. Initially clear when below its activation temperature, the TLC changed colour from red to green to blue as the disc was heated by the hot air entering through the pre-swirl nozzles. The image appears "frozen" because the rotor was illuminated by the stroboscopic light synchronised with the disc rotating at 5000 rpm. The hub and casing (at radii a and b), pre-swirl nozzles, and the blade receiver holes (insulated using low-conductivity, white Rohacell foam) are labeled in the figure. The TLC and overcoat of black paint had been sprayed in a 48° sector on the disc covering eight of the 60 receiver holes. To the left of this painted sector on the rotor, the stator (coated with wide-band TLC) and two of the 24 pre-swirl nozzles are visible through the transparent (unpainted) polycarbonate at low radius. Some shadows appear around the receiver holes due to constraints with the lighting and viewing angles. Both the 30 and 40 °C TLC have been activated into their visible range and display different colours at different locations on the rotating disc. Blue reveals higher temperature, indicating that there is a region of relatively high heat transfer around the receiver holes; the virtually identical colour patterns around each of these holes indicate the circumferential periodicity of the flow structure. Colour images, recorded by a digital video camera running at 25 frames per second, were subsequently converted to hue. As explained in Section 4, it was then possible to determine a hue-time pair at each measurement point on the disc.

A typical example of the variation of the measured total-temperature with time of the pre-swirl 'cooling air' is shown in Fig. 3. The air temperatures were measured using a fast-response total-temperature probe, carefully calibrated for recovery factor (see below). The measurements were made at two locations: the first location is immediately downstream of the mesh heater, and here the temperature can be seen to exhibit a virtual step-change from an initial value of around 20 °C to a final steady-state temperature of 53 °C (see insert); the second location is at the exit of the pre-swirl nozzles, where the air enters the test section. Despite the thermal insulation in the upstream pipes, the air temperature at this latter location rises exponentially from its initial value towards a final steady-state temperature. A three-term exponential fit was used (see Newton et al. (2003)) and the total-temperature, T_a, history at the pre-swirl nozzles (Fig. 3) can be represented by the following:

$$T_a = 23.5 + 7.3\left(1 - e^{\frac{-t}{7.9}}\right) + 6.0\left(1 - e^{\frac{-t}{0.9}}\right) + 16.1\left(1 - e^{\frac{-t}{0.05}}\right) \quad (1)$$

Typically the crystal colour-change times on the disc surface ranged between 1 and 45 s (depending on the local heat flux), and these times can be of similar magnitude to the time constants of the exponential rise in gas temperature.

A conventional total-temperature probe usually contains a thermocouple, the bead of which is located inside a stainless steel tube in which the flow is brought to rest. Such probes have a large recovery factor (≈0.95) but a poor time response. For the tests described here, a K-type bare-wire thermocouple, made from wires of 25 μm diameter, was constructed. The wires were contained inside a stainless steel tube with the bead outside; there was a distance of 3.5 mm (or 140 wire-diameters) between the exposed bead and the tip of the tube. This construction method supported the thermocouple wires but reduced the thermal error resulting from transient conduction from the bead to the tube. The result was a robust probe with a time-constant of less than 40 ms. A wind tunnel was used to carefully calibrate the probe recovery factor, R, as defined

Please cite this article in press as: Kakade, V.U., et al. Accurate heat transfer measurements using thermochromic liquid crystal. Part 2: Application to a rotating disc. Int. J. Heat Fluid Flow (2009), doi:10.1016/j.ijheatfluidflow.2009.04.005

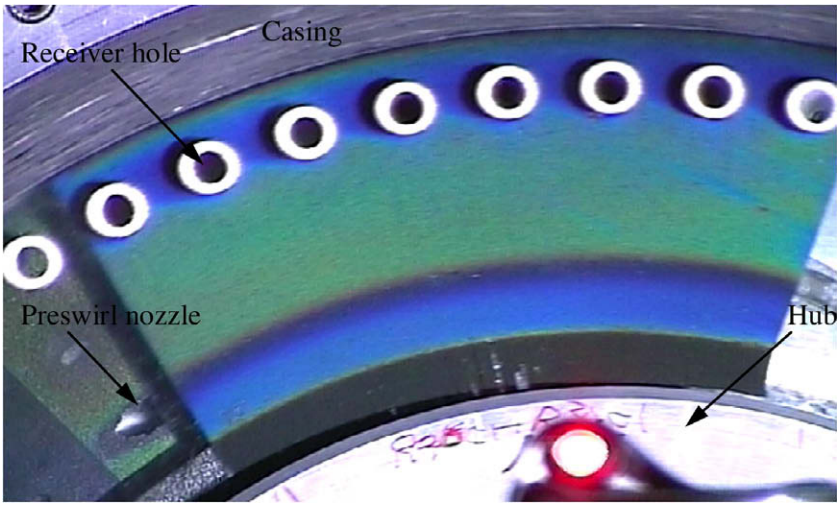

Fig. 2. Photograph of TLC on disc rotating at 5000 rpm.

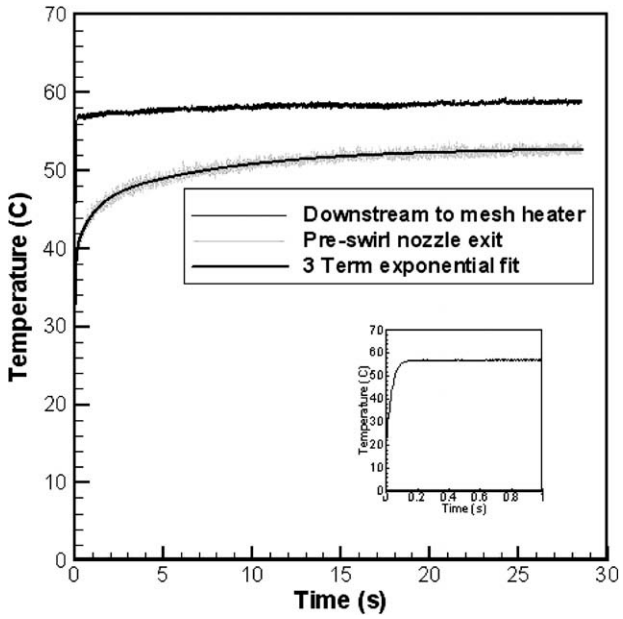

Fig. 3. Typical variation of air temperature with time. The insert shows the air temperature history downstream of the mesh heater over a shorter time scale.

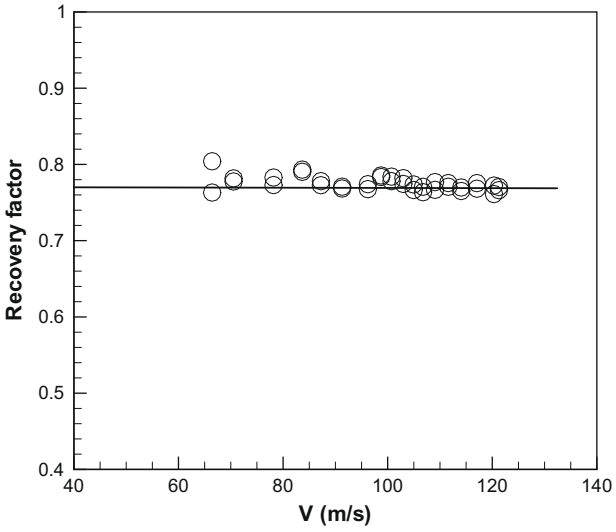

Fig. 4. Recovery factor for fast-response thermocouple.

in Eq. (2), where T_{tc} is the temperature measured by the thermocouple at air velocity V and total temperature T_a.

$$T_a = T_{tc} + (1 - R)\frac{V^2}{2c} \tag{2}$$

The results are shown in Fig. 4, illustrating that for the range of significant air velocities expected in the experiment, $60 < V < 120$ m/s, the recovery factor was constant at $R \approx 0.77$.

3. Data analysis

This section describes briefly the method of analysis for the transient heat transfer experiments based on the solution of Fourier's one-dimensional conduction equation for a semi-infinite substrate as described by Newton et al. (2003). The one-dimensional analysis considers only the conduction in the direction normal to the surface of the wall, ignoring conduction in the transverse directions. Kingsley-Rowe et al. (2005) provide an analytical correction when lateral conduction is significant.

The heat transfer coefficient, h, is defined as

$$q_w = h(T_{aw} - T_w) \tag{3}$$

where q_w is the surface heat flux from the air to the wall, T_w is the surface temperature of the wall, and T_{aw} is the adiabatic-wall temperature. T_{aw} depends on the total-temperature of the air, T_a, and on the fluid dynamics (see Newton et al., 2003).

In a typical transient test, a sudden change in air temperature is generated, and narrow-band TLC is used to determine the surface temperature of the test piece. Knowing the time, t, at which the surface reaches T_w, h (which is assumed to be time-invariant) can be calculated from the solution of Fourier's one-dimensional conduction equation for the case of a semi-infinite plate. In the tests reported here, the mesh heater created an effective step-change in the air temperature, but (as discussed above) at the test section an exponential-type of behaviour (or so-called "slow transient")

Please cite this article in press as: Kakade, V.U., et al. Accurate heat transfer measurements using thermochromic liquid crystal. Part 2: Application to a rotating disc. Int. J. Heat Fluid Flow (2009), doi:10.1016/j.ijheatfluidflow.2009.04.005

was produced. Newton et al. (2003) showed that the adiabatic-wall temperature, T_{aw}, could be fitted by an exponential series of m terms. Fourier's conduction equation for a semi-infinite slab has been solved by Gillespie et al. (1998) for the case where there is a simple exponential increase in the air temperature, corresponding to the case where $m = 1$. The general solution for an exponential series is given by Newton et al. (2003) as

$$\Theta = \sum_{j=1}^{m} \frac{T_{a,j}}{T_{aw,\infty} - T_0} g\left(\beta, \beta_{\tau_j}\right) \tag{4}$$

where

$$g(\beta,\beta_\tau) = 1 - \frac{1}{1+\beta_\tau^2} e^{\beta^2} erfc(\beta) - e^{-t/\tau}\frac{\beta_\tau^2}{1+\beta_\tau^2} \times \left\{1 + \frac{1}{\beta_\tau}\left[\frac{1}{\pi}\sqrt{\frac{t}{\tau}} + \frac{2}{\pi}\sum_{n=1}^{\infty}\frac{1}{n}e^{-n^2/4}\sinh\left(n\sqrt{\frac{t}{\tau}}\right)\right]\right\} \tag{5}$$

$$\beta = \frac{h\sqrt{t}}{\sqrt{\rho c k}} \quad \text{and} \quad \beta_\tau = \frac{h\sqrt{\tau}}{\sqrt{\rho c k}} \tag{6}$$

In summary, T_0, T_w and t are determined by experimental measurement. Once the values of $T_{a,j}$ and τ_j have been determined from the measured air temperature, h can be found from the numerical solution of Eq. (4). This technique requires only a single measurement of surface temperature, and this has the advantage that narrow-band TLC can be used. As stated above, two narrow-band TLC were used to test the accuracy of the measurements.

The measurement uncertainty can be quantified by the method described Owen et al. (2003). A summary of this method and a means of minimising these uncertainties are given in Appendix A. Small uncertainties in the measured temperatures can create large uncertainties in the calculated value of h, and the amplification parameter, Φ_h^*, is defined as the ratio of the relative uncertainty in h to the relative uncertainties in the temperatures. The minimum value of Φ_h^* occurs for $\Theta \approx 0.5$, depending on β_τ, though the variation is relatively small for $0.4 < \Theta < 0.6$. Ideally, this is the range of Θ in which experiments with a single TLC should be conducted if the uncertainties in h are to be kept to a minimum. $\Phi_{h,\min}^*$ increases as β_τ increases, and as λ (where $\lambda = \beta/\beta_\tau = \sqrt{t/\tau}$) decreases. It is therefore advantageous to design an experiment where τ is as small as practicable. Note that for the case of a step-change, $\lambda = \infty$ and $\beta_\tau = 0$. Typical values of Φ, β_τ and Φ_h^* for the experiments with the two crystals (see Table 2) are given in the next section.

The TLC film thickness was 45 μm, which (see Part 1) ensured that the crystal did not significantly deteriorate due to aging. It is also necessary that the film is thin enough that it does not significantly affect the temperature history of the substrate. In the solution to Fourier's equation it is assumed that the thin film temperature is the same as the surface temperature of a semi-infinite insulator and subject to the same heat transfer history. The TLC film will create a bias in the measured heat transfer coefficient as follows:

$$\frac{1}{h_o} = \frac{1}{h} + \frac{\delta x}{k} = \frac{1}{h}\left(1 + \frac{h\delta x}{k}\right) = \frac{1}{h}(1 + Bi) \tag{7}$$

Here δx is a length associated with the TLC film thickness and h_0 is the overall heat transfer coefficient which includes the conduction across the TLC film with conductivity k, and Bi is the Biot number based on the film thickness. It follows that the bias, $\delta h = h - h_0$, is related to Bi by

$$\frac{\delta h}{h} \approx Bi = \frac{h\delta x}{k} \tag{8}$$

A 50 μm film (45 μm of TLC and 5 μm of paint) with an estimated $k \sim 0.2\ \mathrm{W\,m^{-1}\,K^{-1}}$ (Guo et al., 1998) creates a bias of 5% for $h = 200\ \mathrm{W\,m^{-2}\,K^{-1}}$. This is an upper bound on the bias, however, as a 45 μm film of TLC is multilayered and the reflected light from the crystals will be reflected from an effective film thickness less than δx. The bias will affect the experimenter's choice of TLC film thickness, which is a compromise between visibility and aging on one side and bias on the other.

Table 2
Summary of parameters relevant to data shown in Fig.6b, using a single-point calibration at $H = 0.53$ for both the 30 and 40 °C crystal. The uncertainty in wall temperature is $P_T = 0.2$ C, $T_O = 23.5$ C and $T_{aw,\infty} = 52.9$ °C.

TLC (°C)	T_w	Time (s)	Θ	λ_1	λ_2	λ_3	β
30	31.4	3.04	0.27	0.62	1.83	8.05	0.42
40	41.2	23.00	0.60	1.71	5.02	22.1	1.18
TLC (°C)	$\beta_{\tau 1}$	$\beta_{\tau 2}$	$\beta_{\tau 3}$	h (W/m2 K)	Φ_h^*	P_h (W/m2 K)	
30	0.68	0.23	0.05	135	8.7	7.9	
40	0.68	0.23	0.05	138	5.5	5.1	

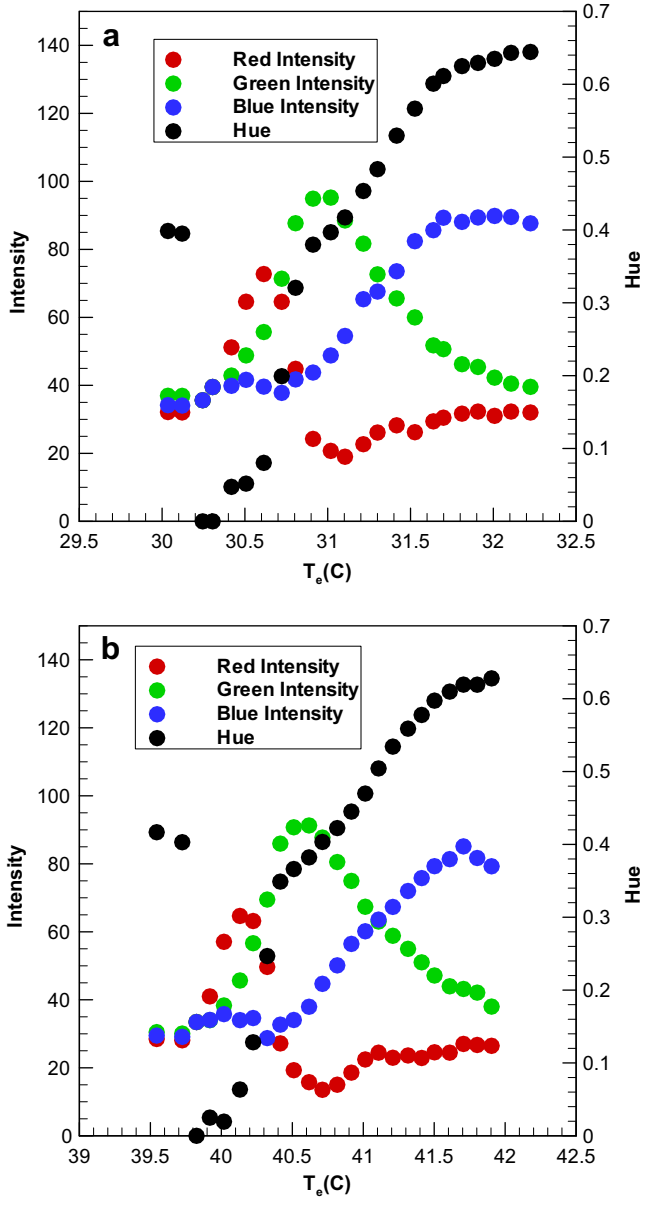

Fig. 5. (a) Calibration curve for 30 °C crystal; (b) calibration curve for 40 °C crystal.

Please cite this article in press as: Kakade, V.U., et al. Accurate heat transfer measurements using thermochromic liquid crystal. Part 2: Application to a rotating disc. Int. J. Heat Fluid Flow (2009), doi:10.1016/j.ijheatfluidflow.2009.04.005

4. Application of calibrated TLC to transient heat transfer experiment

The experimental application uses the 30 and 40 °C crystals specifically calibrated for an indirect view, a lighting angle of 34°, a heating (rather than cooling) cycle, and a film thickness of 45 μm. These calibrations, described in Part 1, were not *in situ* but they do account for the lighting arrangements, optical path, heating and cooling cycles, and peak temperatures expected on the experimental apparatus. In all experimental cases the time of exposure to high temperature was significantly less than the extremes tested in the calibrations, and number of heating cycles experienced by the TLC never created a measureable deterioration in the peak R and G (red and green) intensities. The definitive calibrations are shown in Fig. 5a and b in the form of H, as well as RGB intensity, versus T_e. The uncertainty in the measured temperature is $P_T = 0.2$ °C (note the uncertainty in h is estimated below.)

The experimental method uses these two crystals to identify two particular isotherms (each at a particular calibrated hue) on the test surface at two measured times in the transient experiment. Over the narrow calibrated-temperature range that the crystals are active (~1 °C), a unique value of hue is used for the single-point measurement of wall temperature. With a wide-band TLC, active over (say) 20 °C, it would be possible to use multiple calibrated values of hue to map the surface temperature distribution with time. Unfortunately, the uncertainty in the measurement of surface temperature using the wide-band TLC is an order-of-magnitude greater than that using narrow band, which results in a relatively large uncertainty in h.

The experiment begins with the disc at a known initial temperature, below the activation temperature of both crystals. During the transient, the colour changes of the 30 and 40 °C crystals were recorded as the disc was heated convectively by air at a total temperature ~53 °C. The data were subsequently converted into a series of frames (25 per second) and stored as bitmap using the software Avid Liquid 7.0 in a completely automated manner. Three receiver holes on the disc surface fit into a camera-image area of 450 × 450 pixels. A median filter is used in each 10 × 10 pixel area (corresponding to an area of 0.2 mm × 0.2 mm on the disc) within the image to determine the change of hue with time at each pixel. Fig. 6a ($\lambda_T = 0.12$, $\beta_p = 0.5$, $Re_\varphi = 1 \times 10^6$) shows a typical hue history measured at one location, where the scales of the lower and upper abscissa, measured in frames, differs for the two crystals. The 30 and 40 °C crystals are seen to be active between (approximately) frames 50–100 and 460–700 respectively. Though h is invariant with time, the heat flux at any location decreases with time as the difference between the wall and gas-driving temperature (~53 °C) decreases. The rate of increase of hue is correspondingly greater for the 30 °C crystal.

Fig. 6b shows the data in more detail, with left and right ordinates showing different ranges of H. The value of hue for the single-point calibration of both crystals has been chosen as $H = 0.53$. The time at which this value of H is reached was calculated from the smoothed H-time data, using a range of 10 frames either side of the *reference frame* at which $H \approx 0.53$. A low-pass digital filter and cubic-spline interpolation (marked in the figure) were used for this purpose. In this way, the uncertainty in time was reduced to an insignificant value (‹‹ 40 ms).

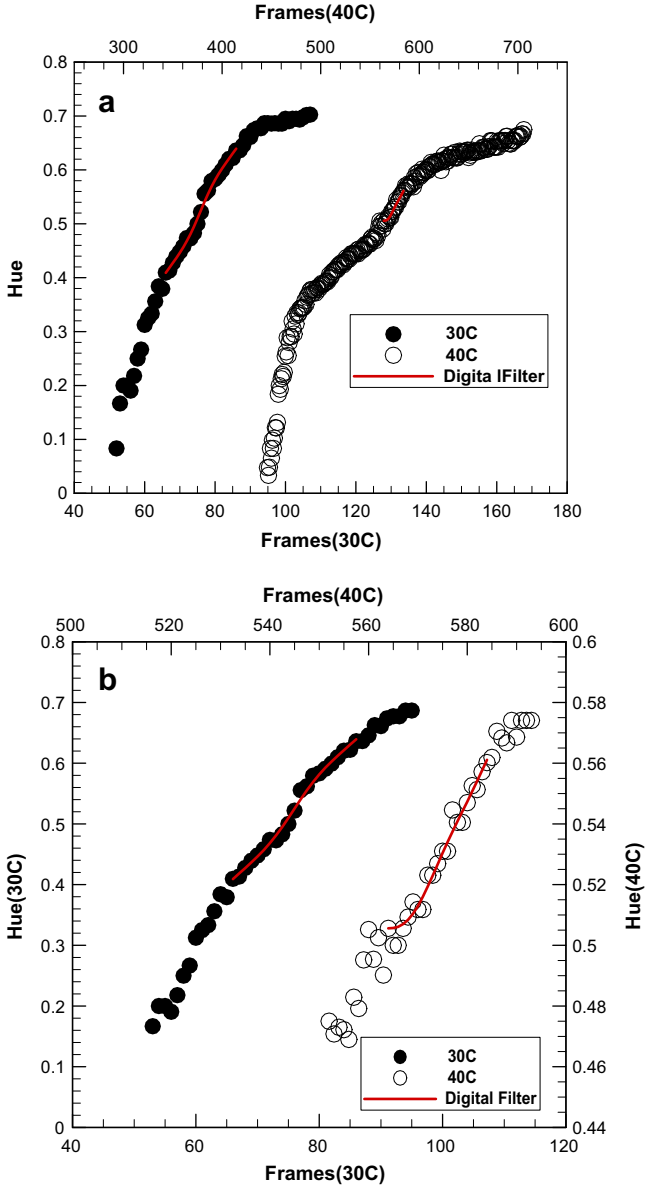

Fig. 6. (a) Variation of hue during transient experiment $\lambda_T = 0.12$, $\beta_p = 0.5$, $Re_\varphi = 1 \times 10^6$; (b) data reduction using low-pass digital filter.

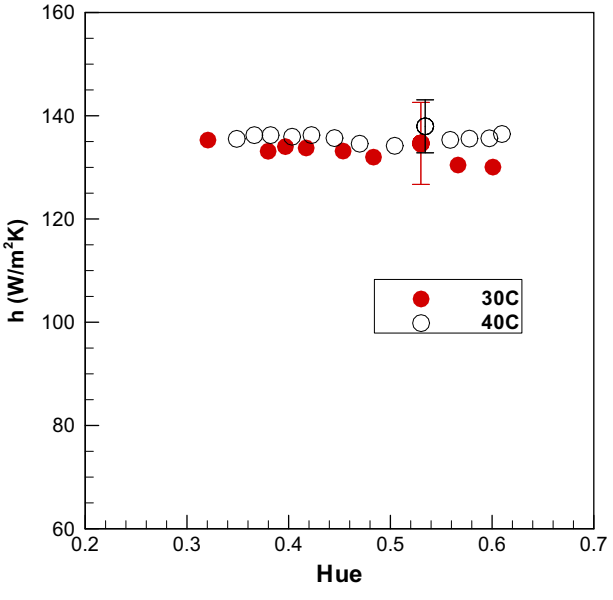

Fig. 7. Variation in heat transfer coefficient with hue $\lambda_T = 0.12$, $\beta_p = 0.5$, $Re_\varphi = 1 \times 10^6$.

Please cite this article in press as: Kakade, V.U., et al. Accurate heat transfer measurements using thermochromic liquid crystal. Part 2: Application to a rotating disc. Int. J. Heat Fluid Flow (2009), doi:10.1016/j.ijheatfluidflow.2009.04.005

The air temperature history for the data in Fig. 6a and b is shown in Fig. 3 and the three-series exponential fit is given by Eq. (1). Table 2 lists the relevant non-dimensional parameters in the solution of Fourier's equation for the data at this pixel. It is noted that the values of Θ, λ and β_τ are sufficiently advantageous to result in acceptable values of Φ_h^* and the uncertainties, P_h, for both crystals. Also the difference between these two values of h, assumed invariant with time, is smaller than the theoretical uncertainties of the measurements.

The choice of H for the single-point calibration was arbitrary. Part 1 has shown that there is an advantage in using $H < 0.38$. Here the variation in the viewing angle across the portion of the disc active with TLC was less than 2° and so a wider range of H was available as a calibration point. There was an advantage in using a

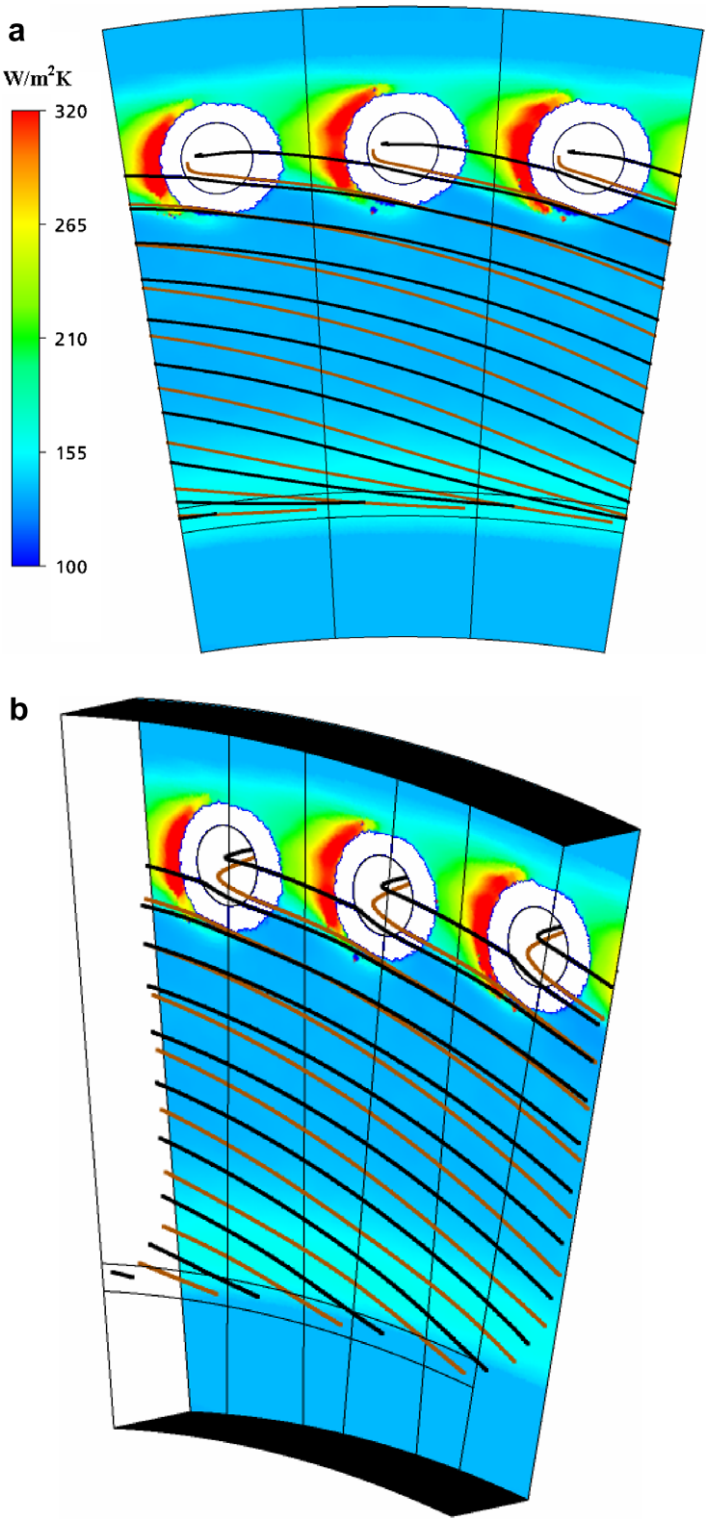

Fig. 8. (a) Measured contours of heat transfer coefficient on the rotating disc (rotating clockwise) with superimposed streamlines – $\lambda_T = 0.12$, $\beta_p = 0.5$, $Re_\varphi = 1 \times 10^6$; (b) measured contours of heat transfer coefficient on the rotating disc (rotating clockwise) with superimposed streamlines – $\lambda_T = 0.12$, $\beta_p = 0.5$, $Re_\varphi = 1 \times 10^6$.

Please cite this article in press as: Kakade, V.U., et al. Accurate heat transfer measurements using thermochromic liquid crystal. Part 2: Application to a rotating disc. Int. J. Heat Fluid Flow (2009), doi:10.1016/j.ijheatfluidflow.2009.04.005

relatively large H because this increased the number of frames before the crystals were activated. In regions of highest heat flux, the reference frame number for the 30 °C crystal could be low enough to create a significant uncertainty in the elapsed time relative to the start of the experiment. Conversely, in regions of low heat transfer a large value of H potentially means that the reference frame number for the 40 °C is beyond the acceptable time limit of the experiment. The time of the experiment is also limited by the semi-infinite wall assumption. Using the conservative criterion (where the substrate temperature at maximum depth changes by <1%) suggested by Schultz and Jones (1973) this time limit was set at approximately one minute for a 10-mm-thick polycarbonate substrate. It is possible to use different values of H for the single-point calibration in different areas of the test piece to optimise the data analysis, but this was considered cumbersome and a single value of $H = 0.53$ was used universally for both crystals.

Fig. 7 shows the value of h determined from the data in Fig. 6b from different calibrated values of H. Both the 30 and 40 °C crystals are shown and it is observed that any value of hue over the range $0.3 < H < 0.6$ provides an equal value of h within experimental uncertainty.

5. Experimental results

Kakade et al. (2009) will report a detailed study investigating the influence of flow rate, swirl ratio, rotational Reynolds number and nozzle location on the heat transfer using the experimental facility described in Section 2. Two heat transfer regimes were observed: a *viscous* regime at relatively low values of λ_T, and an *inertial* regime at high values of λ_T. The viscous regime corresponds to axisymmetric boundary-layer flow over most of the rotating disc. The inertial regime features an impingement on the disc near the pre-swirl nozzle radius with an associated peak in h. In both regimes, three-dimensional flow near the receiver holes on the disc creates non-axisymmetric heat transfer in this region, with large values of h between and around the holes. As the paper here is concerned only with the TLC calibration and application of the transient technique, only a small sample of the experimental data is provided.

Fig. 8a and b are contour maps of heat transfer coefficient on the rotating disc in circumferential section and isometric view, respectively. No data is shown in the immediate vicinity of the receiver holes as these were insulated using Rohacell foam – see Fig. 2. The disc is shown rotating in the clockwise direction and the data is determined from the 40 °C narrow-band TLC. The fluid-dynamic conditions feature a relatively low value of λ_T ($\lambda_T = 0.12$, $\beta_p = 0.5$, $Re_\varphi = 1 \times 10^6$), hence relatively weak impingement from the pre-swirl nozzles, and this viscous-flow regime is dominated by the boundary layer on the rotating disc. The largest levels of h are measured near the receiver holes where three-dimensional flow near the surface of the disc creates a non-axisymmetric distribution of h. Superimposed onto the contours are streamlines of pre-swirl air relative to the rotor calculated from the CFD code CFX (Lewis et al., 2007). Two streamlines of cooling air from the pre-swirl nozzles are used as supporting flow visualisation information. Streamline A (orange) is entrained into the disc boundary layer, continues to a higher radius and then flows out through the receiver hole. Streamline B (black) has a less direct route, impinging onto the downstream side of the hole and forming part of a new boundary layer, eventually exiting through the next (anti-clockwise) receiver hole; this impingement and the associated thin boundary layer gives rise to the crescent-shaped region of high heat transfer on the downstream side of each receiver hole.

Fig. 9a and b show the heat transfer coefficient for fluid-dynamic conditions which feature a relatively high value of λ_T ($\lambda_T = 0.35$, $\beta_p = 1.5$, $Re_\varphi = 1 \times 10^6$), hence relatively high-velocity jets exiting the pre-swirl nozzles; this inertial-flow regime is dominated by impingement on the rotating disc. There is a strong radial variation in h, with the highest levels located at the nozzle radius.

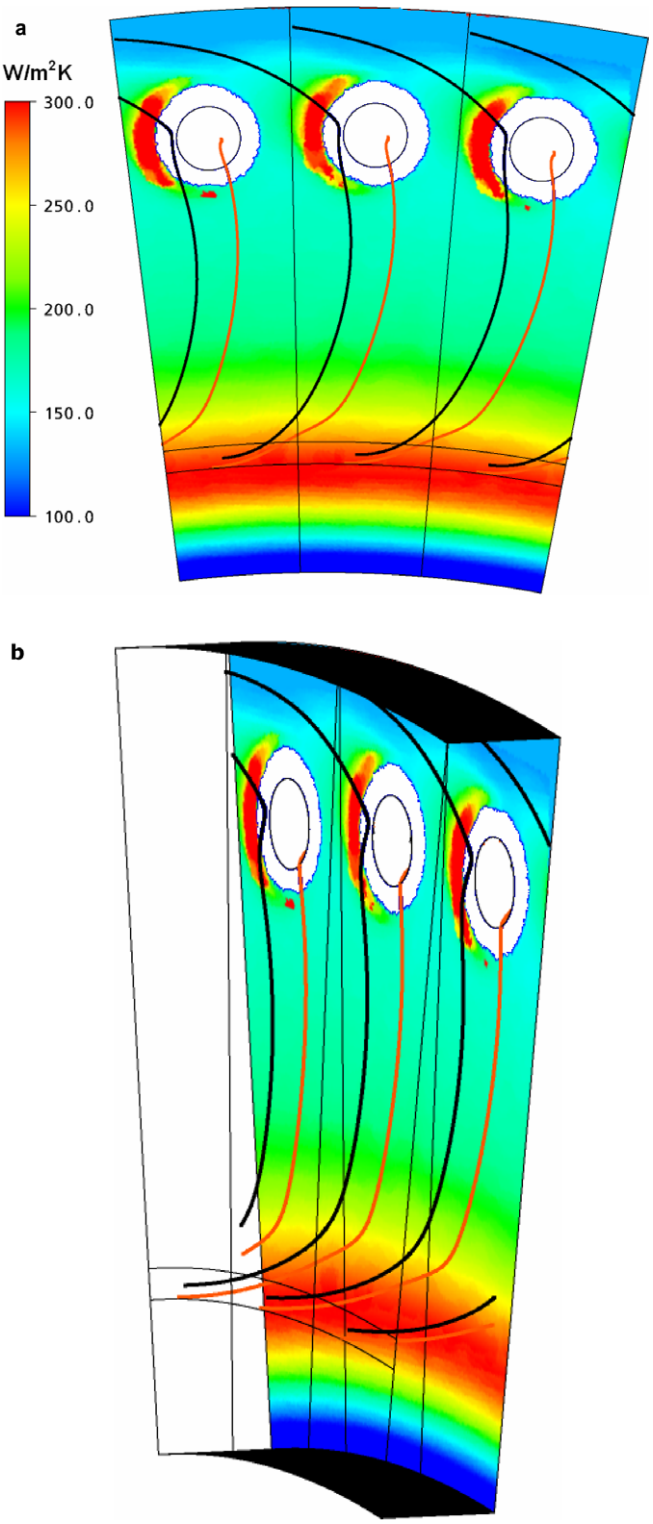

Fig. 9. (a) Measured contours of heat transfer coefficient on the rotating disc (rotating clockwise) with superimposed streamlines – $\lambda_T = 0.35$, $\beta_p = 1.5$, $Re_\varphi = 1 \times 10^6$; (b) measured contours of heat transfer coefficient on the rotating disc (rotating clockwise) with superimposed streamlines – $\lambda_T = 0.35$, $\beta_p = 1.5$, $Re_\varphi = 1 \times 10^6$.

Please cite this article in press as: Kakade, V.U., et al. Accurate heat transfer measurements using thermochromic liquid crystal. Part 2: Application to a rotating disc. Int. J. Heat Fluid Flow (2009), doi:10.1016/j.ijheatfluidflow.2009.04.005

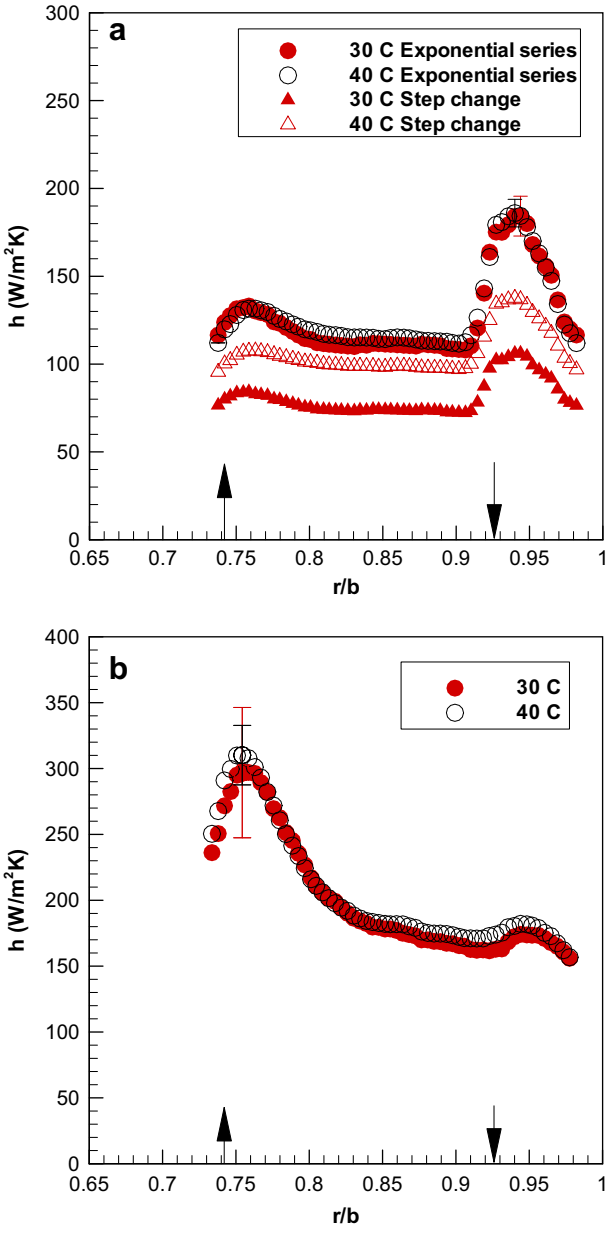

Fig. 10. (a) Radial variation of heat transfer coefficient determined from both 30 and 40 °C crystals for viscous regime – $\lambda_T = 0.12$, $\beta_p = 0.5$, $Re_\varphi = 1 \times 10^6$. Uncertainty bars also shown. Data for both step-change and exponential series is shown. (b) Radial variation of heat transfer coefficient determined from both 30 and 40 °C crystals for inertial regime – $\lambda_T = 0.35$, $\beta_p = 1.5$, $Re_\varphi = 1 \times 10^6$. Uncertainty bars also shown.

High levels of h are also measured adjacent to the receiver holes where the three-dimensional flow near the surface of the disc creates a non-axisymmetric distribution of h. As in Fig. 8a and b, streamlines are superimposed onto the contours. Streamline A (orange) is entrained into the disc boundary layer, continues to a higher radius and then flows out through the receiver hole. Streamline B (black) impinges onto the downstream side of the hole, forming part of a new boundary layer, then continues to a higher radius where it will recirculate into the system and mix with the core flow (i.e. the region outside the stator and rotor boundary layers). As in the viscous regime, the impingement and associated thin boundary layer gives rise to the crescent-shaped region of high heat transfer on the downstream side of each receiver hole.

Fig. 10a and b show the variation in h, determined using both the 30 and 40 °C crystals, with non-dimensional radius (r/b) along a line midway between two receiver holes. The pre-swirl inlet and receiver-hole exit locations are marked by arrows in the figures. In Fig. 10a the values of h determined from a step-change solution (rather than the exponential-series solution) to $T_{aw,\infty}$ for the two crystals is also shown. The step-change solution underestimates h and the values determined by the two crystals differ significantly. The close agreement between the two data sets determined by the exponential-series solution illustrates the accuracy of the experiments and validates the calibration and method of analysis. The maximum uncertainties, as determined by the method of Owen et al. (2003), are also shown in these figures. Kingsley-Rowe et al. (2005) provide an analytical correction when lateral conduction is significant. This analysis was applied to the experiments reported here though the corrections were well within the bounds of experimental uncertainty.

6. Conclusions

Liquid crystals are a powerful tool for studying heat transfer and fluid-flow experiments. Accurate experimental measurements of heat transfer coefficient, h, depend on the following: appropriate choice of the activation ranges of the crystals; careful calibration of the crystals for the conditions that will be experienced in the experiments; judicious smoothing and filtering of the hue-time data; appropriate exponential-fitting of the air temperature–time data (unless a step-change can be achieved!); and an accurate solution of Fourier's equation. In addition, the use of two different crystals is strongly recommended: they provide confidence in the accuracy of the measurements. If all of these conditions are satisfied, experimental uncertainties in h can be minimised and the TLC technique can provide a wealth of qualitative and quantitative information.

In this paper, two narrow-band liquid crystals were used to measure the surface temperature on a rotating disc in a transient experiment which models the flow of internal cooling in a gas turbine. The convective heat transfer coefficient was subsequently calculated from the solution of Fourier's conduction equation and accounted for the exponential rise in the air temperature driving the heat transfer. The relevant non-dimensional parameters in the solution (Θ, λ and β_τ) were sufficiently advantageous to result in low uncertainties in measured h for both crystals. The experiments revealed two heat transfer regimes: a viscous regime at relatively low coolant flow rates, and an inertial regime at higher flow rates. Both regimes featured regions of high heat transfer where new, thin, boundary layers replaced air exiting though holes at high radius on the rotating disc.

The calibration methods, exponential-series technique, and uncertainty analysis presented in this paper could be used successfully in many transient experiments, regardless of whether the surface viewed is stationary or rotating, and particularly in applications for which it is not possible to achieve a satisfactory step-change in air temperature at the test section.

Acknowledgements

Dr James Mayhew participated in this research while on sabbatical from Rose-Hullman Institute of Technology between September 2006 and March 2007.

Appendix A. Experimental uncertainties

The uncertainty in h for the "slow transient" technique was quantified by Owen et al. (2003), and a summary is given here.

Small uncertainties in the measured temperatures can create large uncertainties in the calculated value of h, and the amplification parameter, Φ_h^*, is defined as the ratio of the relative uncertainty in h to the relative uncertainties in the temperatures. For the special case when the uncertainties in all measured temperatures are equal, Φ_h^* is determined from the weighted components of the exponential series of j terms:

$$\Phi_h^{*-1} = \sum_{j=1}^{m} c_j \Phi_{h,j}^{*-1}$$

where

$$\Phi_{h,j}^* = \Gamma_\Theta^* \Gamma_{\beta j} \quad \Gamma_\Theta^* = \left\{2\left(1 - \Theta + \Theta^2\right)\right\}^{\frac{1}{2}} \quad \Gamma_{\beta,j}^{-1} = \beta \frac{\partial}{\partial \beta}\left[g(\beta, \lambda_j)\right].$$

The variables Θ and $g(\beta, \lambda)$, β and β_τ are defined by Eqs. (4)–(6), and

$$\lambda_j = \frac{\beta}{\beta_{\tau j}} = \sqrt{\frac{t}{\tau_j}} \quad \text{with} \quad c_j = \frac{T_{aj}}{\sum_{j=1}^{m} T_{aj}}.$$

The effect of λ on the variation of Φ_h^* with Θ is shown in Owen et al. (2003). Φ_h^* for the exponential case is larger that than for the step-change and, for small values of λ, it can be very large. For example, for $\lambda = 0.4$, $\Phi_h^* > 35$: 1% uncertainty in temperature results in more than 35% uncertainty in h. It is therefore desirable to make λ as large as practicable so as to reduce the uncertainty in h. For any value of λ, there is an optimum value of Θ that will minimise Φ_h^*, and this optimum value increases as λ increases: for $\lambda > 2$, $\Theta_{\text{opt}} \approx 0.52$. As τ is dependent on the experimental apparatus, the experimenter needs to choose both λ and Θ so as to achieve acceptably small values of Φ_h^* for the duration of the experiment.

The effect of β_τ on the variation of Φ_h^* with Θ is shown in Owen et al. (2003). The step-change case (where $\beta_\tau = 0$) provides the lower bound for Φ_h^*, and this limit is approached for $\beta_\tau < 1$. The minimum value of Φ_h^* occurs for $0.5 < \Theta < 0.6$, depending on β_τ, and this is the range of Θ in which experiments with TLC should be conducted if the uncertainties in h are to be kept to a minimum. $\Phi_{h,\min}^*$ increases as β_τ increases: for $\beta_\tau = 1$, $\Phi_{h,\min}^* \approx 5$; for $\beta_\tau = 10$, $\Phi_{h,\min}^* \approx 23$. It therefore makes sense to design an experimental rig that makes τ as small as practicable, and to choose crystals that ensure Θ is in an acceptable range.

References

Baugh, J.W., 1995. Liquid crystal methods for studying turbulent heat transfer. Int. J. Heat Fluid Fl. 16, 365–375.

Cardone, G., Astarita, T., Carlomagno, G.M., 1997. Heat transfer measurements on a rotating disk. Int. J. Rotating Mach. 3 (1), 1–9.

Dryer, M., Moller, T.J., Radespiel, R., 2005. Wind tunnel validation experiments to investigate the flow over a rotating and heated disk passed by a planar air stream. In: 21st International Congress on Instrumentation in Aerospace Simulation Facilities, pp. 293–298.

Gillespie, D.R.H., Wang, Z., Ireland, P.T., 1998. Full surface local heat transfer coefficient measurements in a model of an integrally cast impingement cooling geometry. J. Turbomach. 120, 92–99.

Guo, S.M., Lai, C.C., Jones, T.V., Oldfield, M.L.G., Lock, G.D., 1998. The application of thin-film technology to measure turbine-vane heat transfer and effectiveness in a film-cooled, engine-simulated environment. Int. J. Heat Fluid Fl. 19, 594–600.

Ireland, P.T., Jones, T.V., 2000. Liquid crystal measurements of heat transfer and surface shear stress. Meas. Sci. Technol. 11, 969–986.

Kakade, V.U., Lock, G.D., Wilson, M., Owen, J.M., Mayhew, J.E., 2009. Heat transfer in a pre-swirl rotating-disc system. ASME paper GT-2009-59090.

Karabay, H., Wilson, M., Owen, J.M., 2001. Predictions of effect of swirl on flow and heat transfer in a rotating cavity. Int. J. Heat Fluid Fl. 22, 143–155.

Kingsley-Rowe, J., Lock, G.D., Owen, J.M., 2005. Transient heat transfer measurements using liquid crystal: lateral-conduction error. Int. J. Heat Fluid Fl. 26, 256–263.

Lewis, P.R., Wilson, M., Lock, G.D., Owen, J.M., 2007. Physical interpretation of flow and heat transfer in pre-swirl systems. ASME J. Eng. Gas Turb. Power 129, 769–777.

Lock, G.D., Wilson, M., Owen, J.M., 2004. Influence of fluid-dynamics on heat transfer in a pre-swirl rotating-disc system. ASME J. Eng. Gas Turb. Power 127, 791–797.

Mori, M., Novak, L., Sekavcnik, M., 2007. Measurements on rotating blades using IR thermography. Exp. Therm. Fluid Sci. 32 (2), 387–396.

Newton, P.J., Yan, Y., Stevens, N.E., Evatt, S.T., Lock, G.D., Owen, J.M., 2003. Transient heat transfer measurements using thermochromic liquid crystal. Part 1: An improved technique. Int. J. Heat Fluid Fl. 24 (1), 14–22.

Owen, J.M., Rogers, R.H., 1989. Flow and Heat Transfer in Rotating Disc Systems. Rotor–Stator Systems, vol. 1. Research Studies Press, Taunton, UK/Wiley, New York.

Owen, J.M., Newton, P.J., Lock, G.D., 2003. Transient heat transfer measurements using thermochromic liquid crystal. Part 2: Experimental uncertainties. Int. J. Heat Fluid Fl. 24 (2), 3–28.

Pellé, J., Harmand, S., 2007. Heat transfer measurements in an opened rotor–stator system air-gap. Exp. Therm. Fluid Sci. 31 (3), 165–180.

Schultz, D.L., Jones, T.V., 1973. Heat transfer measurements in short duration hypersonic facilities. Agardograph 165.

Yan, Y., Owen, J.M., 2002. Uncertainties in transient heat transfer measurements with liquid crystal. Int. J. Heat Fluid Fl. 23, 29–35.

Yan, Y., Farzeneh Gord, M., Lock, G.D., Wilson, M., Owen, J.M., 2003. Fluid dynamics of a pre-swirl rotating-disc system. ASME J. Turbomach. 125, 641–647.

Please cite this article in press as: Kakade, V.U., et al. Accurate heat transfer measurements using thermochromic liquid crystal. Part 2: Application to a rotating disc. Int. J. Heat Fluid Flow (2009), doi:10.1016/j.ijheatfluidflow.2009.04.005